Target-specific delivery of oxaliplatin to HER2-positive gastric cancer cells *in vivo* using oxaliplatin-au-fe3o4-herceptin nanoparticles

DAREN LIU[1*], XIAOWEN LI[1*], CHANGLEI CHEN[2], CHAO LI[1], CHUANBIAO ZHOU[1], WEIDONG ZHANG[1], JIANGANG ZHAO[1], JIE FAN[2], KAI CHENG[3] and LI CHEN[1]

[1]Department of General Surgery, Second Affiliated Hospital, College of Medicine; [2]Key Laboratory of Applied Chemistry of Zhejiang, Department of Chemistry, Zhejiang University, Hangzhou, Zhejiang 310009, P.R. China; [3]Molecular Imaging Program, Canary Center for Cancer Early Detection, Department of Radiology and Bio-X Program, Stanford University, Stanford, CA 94305, USA

Received April 18, 2016; Accepted December 14, 2017

DOI: 10.3892/ol.2018.8323

Abstract. Gastric cancer is the fourth most common malignancy globally. In order to decrease the dosage and side effects of conventional chemotherapy, and achieve improved benefits from molecular targeted therapy, novel drug delivery systems were developed in the present study. Oxaliplatin-Au-Fe_3O_4-Herceptin® acts as a dual-functional nanoparticles (NPs) conjugate and possesses the capability of human epithelial growth factor receptor 2 (HER2) targeting and oxaliplatin delivery. The 8-20 nm Au-Fe_3O_4 were synthesized by decomposing iron pentacarbonyl on the surfaces of Au NPs in the presence of oleic acid and oleylamine. Following being coated with polyethylene glycol, the NPs possessed a ζ-potential of 13.8±1.6 mV and were demonstrated to exhibit no cytotoxicity when Fe concentration is <100 μg/ml via an MTS assay. Mass spectrometry analysis detected a peak at *m/z* 148,000, and Nuclear Magnetic Resonance indicated peaks at δ 3.51 (8.00H, s, 3-H), 2.97-3.02 (3.80H, t, 2-H) and 2.72-2.76 (3.72H, t, 1-H) following successful loading with Herceptin and oxaliplatin probes. A drug release assay via dialysis cassettes demonstrated that 25% of the oxaliplatin was released at pH 8.0, however >58% was released at pH 6.0 following 4 h incubation, indicating its pH-dependent release characteristic. The active targeting feature of oxaliplatin-Au-Fe_3O_4-Herceptin was verified in a subcutaneous xenograft mouse model containing SGC-7901 cells via detecting aggregated low intensity in T_2-weighted magnetic resonance imaging, which was further confirmed by immunohistochemistry. Therefore, oxaliplatin-Au-Fe_3O_4-Herceptin is a promising multifunctional platform for simultaneous magnetic traceable and HER2 targeted chemotherapy for gastric cancer.

Correspondence to: Professor Li Chen, Department of General Surgery, Second Affiliated Hospital, College of Medicine, Zhejiang University, 88 Jiefang Street, Hangzhou, Zhejiang 310009, P.R. China
E-mail: chenli@mail.hz.zj.cn

*Contributed equally

Key words: Au-Fe_3O_4, nanoparticles, Herceptin, oxaliplatin, drug release, gastric carcinoma

Introduction

Gastric cancer is the fourth most common malignancy and accounts for >740,000 cancer-associated mortalities/year globally (1,2). Despite great improvements made in therapeutic methods in recent years, the prognosis is still unsatisfactory (3). Novel combinations of conventional chemotherapies, including the SPIRITS trial (S1 plus cisplatin vs. S1) demonstrated improved overall survival in patients treated with S1 plus cisplatin (13.0 months) compared with those treated with S1 alone (11.0 months) (4). Additionally, other combinations of cytotoxic agents, including docetaxel, irinotecan, capecitabine and oxaliplatin, have also been reported to prolong survival. However, therapeutic efficacy is still limited by two major factors: Drug resistance and side effects (5-7).

Human epithelial growth factor receptor 2 (HER2) is over-expressed in a significant proportion of gastric cancers (6-23%) (8). It is associated with tumor invasion, metastasis, chemoresistance and poor prognosis (9). Trastuzumab, as a recombinant humanized monoclonal antibody that targets the extracellular domain IV of HER2, is one of the most promising targets in human malignancy in recent years (10). In trial investigating the use of trastuzumab for gastric cancer, the addition of trastuzumab (Herceptin®) to chemotherapy significantly improved overall survival (13.8 months, 95% CI 12-16) compared with chemotherapy alone (11.1 months, 95% CI 10-13) in patients with HER2-positive gastric cancer (11), which indicated that combined chemotherapy with trastuzumab may be a novel treatment for patients with HER2-positive advanced gastric cancer. However, the majority of patients with gastric cancer still develop acquired resistance to trastuzumab (12). To achieve improved benefits for HER2-targeted therapy, the development of novel drug delivery systems that may decrease

the dosage and periods of molecular targeted therapy are urgently required.

Nanoparticle (NP)-based therapeutics offer an innovative method to overcome the limitations of current agents (13). NPs possess unique properties that enable them to be used as imaging probes, which may be traced via magnetic resonance imaging (MRI) and therapeutic agents at the same time (14); however, they can be further loaded to deliver specific drugs (15-16) or target specific molecules (17,18). Superparamagnetic iron oxide (SPIO), known to be a highly efficient T_2 contrast agent for MRI, is an ideal small molecular probe for medical use (19). Although SPIO exploit an enhanced permeability and retention effect (EPR) for tumor uptake, EPR is still inefficient with relatively low concentrations of NPs reaching tumors (20). Vascular heterogeneity commonly exists in large tumors, particularly metastases, and leads to unpredictable rates of NP extravasation as well as decreased perfusion and overall uptake (21,22). Therefore, the development of active targeting NPs is required. However, reports on SPIO with a combined feature of targeted intracellular drug release and imaging function are rare.

In the present study, a dual-functioning NPs conjugate, Au-Fe_3O_4, for HER2 targeted oxaliplatin delivery and intracellular drug release triggered via pH, was developed. In order to illustrate its targeting and therapeutic potential, cell culture and animal experiments of oxaliplatin-Au-Fe_3O_4-Herceptin NPs against human gastric cancer cell line SGC-7901 were conducted. It was demonstrated in the present study that selective targeting of HER2-positive gastric cancer cells using oxaliplatin-Au-Fe_3O_4-Herceptin NPs may increase the efficacy and decrease the side effects of oxaliplatin chemotherapy.

Materials and methods

Preparation of Au-Fe_3O_4 NPs modified with poly(ethylene glycol) (PEG). For typical synthesis of 8 nm Au NPs, a precursor solution containing hexane (10 ml), oleylamine (10 ml) and 0.1 g of $HAuCl_4{\cdot}_4H_2O$ (Aladdin Shanghai Biochemical Technology Co., Ltd., Shanghai, China) was prepared and magnetically stirred at 15˚C under low flow N_2 (15˚C, 15 MPar). Following 10 min, a premixed solution (at 15˚C) containing tetrabutylammonium bromide (0.5 mmol), hexane (1 mmol) and oleylamine (1 mmol) was injected into the precursor solution; the solution changed color to deep purple within 5 sec. The mixture was incubated at 15˚C for 1 h prior to the precipitation by absolute ethyl alcohol. The precipitated Au NPs were collected by centrifugation (11,688 x g, 8 min), dissolved in absolute ethyl alcohol and detected via transmission electron microscope (TEM; JEOL 1230; JEOL, Ltd., Tokyo, Japan) at 80-200 kV.

Au NPs (0.48 mmol), octadecene (20 mmol), oleic acid (8 mmol) and oleylamine (8 mmol) were then mixed prior to adding iron acetylacetonate (6 mmol) and dodecanediol (20 mmol) into the solution at 180˚C for 2 h followed by 300˚C for 1 h. Following cooling to room temperature, Au-Fe_3O_4 NPs were collected by centrifugation (16,501 x g, 10 min) and detected via TEM at 80-200 kV.

Surface modification of Au-Fe_3O_4 NPs. For Au-Fe_3O_4 modification, 50 ml α,ω-Bis{2-[(3-carboxy-1-oxopropyl) amino]ethyl}PEG (M_r=2,000; Sigma-Aldrich; Merck KGaA, Darmstadt, Germany), 1.0 mg of N-hydroxysuccinimide (NHS; Sigma-Aldrich; Merck KGaA), 1.25 g of dicyclohexylcarbodiimide (Aladdin Shanghai Biochemical Technology Co., Ltd., Shanghai, China) and 1.5 g of dopamine hydrochloride were dissolved in a mixture of $CHCl_3$ (20 mmol), dimethylformamide (8 mmol) and anhydrous Na_2CO_3 (6 mmol). The solution was stirred at 37˚C for 2 h, Au-Fe_3O_4 NPs (5 mg) were added, and the resulting solution was stirred overnight at 37˚C under a N_2 flow. The modified NPs were precipitated by adding cyclohexane (25 mmol), collected by centrifugation at 16,501 x g, dried under N_2 flow at 40˚C (23). Surfactants and other salts were removed via dialysis (molecular mass cut off, 14,000 kDa; Spectrum Laboratories, Inc., Rancho Dominguez, CA, USA) for 24 h in PBS or water. The final iron concentration of the particles was determined by inductively coupled plasma mass spectrometry (ICP-MS; Element XR, Thermo Fisher Scientific, Inc., Waltham, MA, USA), which is a type of mass spectrometry capable of detecting metals and several non-metals at concentrations as low as one part in 10^{15} (part/quadrillion) on non-interfered low-background isotopes. The ICP multi-element standard solution IV (1,000 mg/kg, Merck KGaA, Darmstadt, Germany) was used as background equivalent concentration in the ICP-MS measurement. The nitric acid (HNO3) and hydrochloric acid (HCl) used were ultra-pure 100 grade (Merck KGaA). High purified water was obtained by a Milli-Q system (Merck KGaA). The operating conditions of ICP-MS are listed in Table I.

Conjugation of Herceptin and oxaliplatin to Au-Fe_3O_4 NPs. To conjugate the anti-HER2 antibody Herceptin, Au-Fe_3O_4 NPs in methyl ester sulfonate (Aladdin Shanghai Biochemical Technology Co., Ltd.) were mixed with 1-ethyl-3-(3-dimethylaminopropyl) carbodiimide (EDC; Sigma-Aldrich; Merck KGaA) for 15 min at 4˚C. Sulfo-NHS (Sigma-Aldrich; Merck KGaA) was added into the solution, which was then subjected to PD-10 column (GE Healthcare Life Sciences, Uppsala, Sweden) filtering to remove excessive EDC and sulfo-NHS, according to the manufacturer's protocol. Herceptin (Genentech Inc., San Francisco, CA, USA) was added into the conjugate following the alteration of pH to 7.4. The antibody-conjugated NPs were separated from unbound Herceptin and Au-Fe_3O_4 NPs using 300 K ultra-filtration (Optima MAX-TL, Beckman Coulter, Inc., Brea, CA, USA). The peptide bond of Au-Fe_3O_4-Herceptin was recorded by infrared (IR) spectroscopy on a Nicolet™ iS10 spectrometer (Thermo Fisher Scientific, Inc.) in the range between 2,500-400 cm^{-1} and a resolution of 2 cm^{-1}. The Herceptin mass spectrum was detected by matrix-assisted laser-desorption ionization/time-of-flight (TOF)/TOF using Ultraflex III TOF/TOF MS (Bruker-Michrom, Inc., Auburn, CA, USA). MALDI-TOF MS measurements were taken using reflectron positive-ion mode. Acceleration was performed at 25 kV. Laser power was set as high as possible allowing baseline separation of isotopic peaks. Sample spectra were acquired by summing 25,000 laser shots at a frequency of 2,000 Hz, using a window from m/z 2,000 to 20,000 (Table II). To confirm the structures of the peaks, tandem mass spectrometry (MALDI-TOF/TOF MS/MS) was performed using laser-induced disassociation. Data acquisition was performed with the FlexImaging 3.0 software (Bruker-Michrom, Inc.).

Table I. Operating conditions of ICP-MS.

Parameter	Setting
Radio frequency power	1300 W
Plasma gas flow rate	16 l/min
Auxiliary gas flow rate	0.85 l/min
Carrier gas flow rate	1.12 l/min
Nebulizer	Micromist nebulizer with uptake rate of 200 l/min
Spray chamber	Isomist spray chamber
Sampling cone	1.0 mm
Skimmer cone	0.7 mm
Sampling depth	2.6 mm
Replicate of mesurement	5 times
Measured element and resolution mode ($m/\Delta m$)	^{57}Fe (4000), ^{195}Pt (4000)

Table II. Operating conditions of MALDI-TOF MS.

Parameters	Settings
Mode	Reflectron positive-ion mode
Laser	200 Hz smartbeam-I laser
Delay	80 ns
Ion source	1 voltage, 25 kV; 2 voltage, 23.4 kV
Lens voltage	6 kV
Mass range	2,000-20,000 kDa
Software	FlexImaging 3.0 software (Bruker-Michrom, Inc.)

Table III. Chromatographic conditions.

Parameters	Settings
Column	SiliaFLASH™
Sample volume	8 ml
Band length	6 mm
Application rate	10 s/μl
Scanner	Camag TLC scanner III
Scanning speed	20 mm/s
Data resolution	100 μm/step
Measurement mode	Absorption
Flow rate	10 ml/min
Pressure	8 psi

For oxaliplatin-binding ligand synthesis, ethyl bromoacetate (8 mmol) and KI (3 mmol) were added to a solution of cystamine dihydrochloride (1.125 g, 5 mmol) in 100 ml acetone and 10 ml Et_3N, stirred for 6 h at room temperature and the insoluble solid was removed via filtration. The filtrated crude products was dried and purified on a Biotage flash chromatography (Isolera™, Biotage Inc. Uppsala, Sweden) with SiliaFLASH™ cartridges (SiliCycle Inc. Quebec City, Canada) according to the manufacturer's protocol (24). An appropriate solvent mixture (petrol/EtOAc, 3:1) was used as eluent, obtaining a yield of ~80% (Table III). The carboxylic groups were deprotected in methanol solution (0.496 g, 1 mmol), 5 ml of 1 M NaOH aqueous solution was added, stirred for 30 min at room temperature and a small amount of water was added if any precipitate remained. Following 24 h of stirring, 20 ml distilled water was added, the solution was acidified to pH 3.0 using 1 M HCl and the resulting precipitate was collected by centrifugation (16,501 x g) at 37˚C and washed with EtOH/H_2O (1:1). The detection of ligands of antibody-coupled Au-Fe_3O_4 NPs was preceded by nuclear magnetic resonance (NMR; Bruker Advance 2B/400 MHz; Bruker Corporation).

The antibody-coupled Au-Fe_3O_4 NPs (1 mg) were mixed with oxaliplatin binding ligand solution (described previously) for 6 h at room temperature, uncoupled ligands were removed using a PD-10 column. Oxaliplatin (20 mg/ml; Eloxatin; Sanofi S.A., Paris, France) was added to the NP solution, stirred overnight at room temperature in the dark and unconjugated oxaliplatin was removed via low speed centrifugation (12,000 x g) followed by purification on a PD-10 column. The amount of oxaliplatin bound to the NPs was determined via ICP-MS under the same experimental conditions as previously stated (Element XR, Thermo Fisher Scientific, Inc.).

Oxaliplatin release assay. Oxaliplatin-Au-Fe_3O_4-Herceptin NPs (50 μg/2 ml) were placed into Slide-A-Lyzer™ Dialysis Cassettes (molecular mass cut off, 2,000 kDa; Thermo Fisher Scientific, Inc.), which was in 30 ml PBS at room temperature. At the time intervals of 1, 2, 4, 8 and 19 h, 1 ml PBS was sampled. The platinum concentration was determined via Element XR ICP-MS (Thermo Fisher Scientific, Inc.) additional details can be found in Table I.

Cell lines and animals. Stomach adenocarcinoma cell line SGC-7901 was purchased from American Type Culture Collection (Manassas, VA, USA). SGC-7901 cells were cultured in RPMI-1640 medium (Hangzhou Gino Biomedical Technology Co., Ltd., Hangzhou, China) supplemented with 10% fetal bovine serum (FBS; Hangzhou Sijiqing Biological Engineering Materials, Co., Ltd., Hangzhou, China) and 1% penicillin/streptomycin (Genom Biologic). Cells were incubated in a standard humidified incubator in 5% CO_2 at 37˚C and passaged every 3-5 days using trypsin-EDTA (Genom Biologic). A total of 50, 4-6-week-old female BALB/c nu/nu mice (18-22 g, Shanghai Institutes for Biological Sciences, Shanghai, China) used in the present study were housed 5 to a cage under pathogen-free conditions and maintained on a daily 12/12 h light/dark cycle at Zhejiang University Laboratory Animal Center (Hangzhou, China), a fully accredited Association for Accreditation of Laboratory Animal Care facility. Animals were housed in a sterile environment, fed sterilized food and water *ad libitum*. All animal studies were carried out in strict accordance with the guidelines for the welfare and use of animals in cancer research of the Committee of the National Cancer Research Institute. The Zhejiang University Animal Research Committee approved

the present study protocol. All surgery was performed under sodium pentobarbital anesthesia (40 mg/kg), and all efforts were made to minimize suffering (25). Animal health and behavior was monitored every 12 h, and were euthanized when the mice display early markers associated with mortality or a poor prognosis, including abdominal distension, emaciation or cachexy.

Cell viability assay (cytotoxicity assay). The cytotoxicity of NPs on SGC-7901 was determined using MTS assays (26). Briefly, SGC-7901 cells ($4x10^3$ cells/well) were seeded into 96-well plates and incubated overnight at 37˚C. Au-Fe_3O_4 NPs with different Fe concentrations (0, 50, 100, 150, 200 and 250 mg/l) were added to the designed wells and incubated at 37˚C for 24, 48 and 72 h. Following incubation at 37˚C with MTS solution (CellTiter96®AQ_{ueous} One Solution Cell Proliferation Assay, Promega Corporation, Madison, WI, USA) for 2 h, the absorbance was measured using a TU-1901 Ultraviolet-Visible Spectrophotometer (Beijing Purkinje General Instrument, Co, Ltd., Beijing, China) at 570 nm. The same method was used to measure the cytotoxicity of Au-Fe_3O_4-Herceptin and oxaliplatin-Au-Fe_3O_4-Herceptin at Fe concentrations of 0, 30, 50, 80 and 100 mg/l.

Cellular internalization of NPs. Oxaliplatin-Au-Fe_3O_4-Herceptin NPs with 0.01 mg/ml Fe were added to SGC-7901 cells until they were 70% confluent, cultured with RPMI-1640 medium (10% FBS, 1% penicillin) and incubated for 2 h at 37˚C. Cells ($1x10^5$/ml) were plated on sterile glass slides were first fixed with 2.5% glutaraldehyde (Aladdin Shanghai Biochemical Technology Co., Ltd.) in phosphate buffer (pH 7.0, Aladdin Shanghai Biochemical Technology Co., Ltd.) for 4 h and then with 1% OsO_4 (Aladdin Shanghai Biochemical Technology Co., Ltd.) in phosphate buffer (pH 7.0) for 1 h at room temperature. The specimens were placed in a 1:1 mixture of absolute acetone and Spurr's resin (AGAR Scientific, Ltd., Stansted, UK) for 1 h at room temperature, then placed in capsules contained embedding medium (Sigma-Aldrich; Merck KGaA) and heated at 70˚C for 9 h. The specimen sections of cells were stained with uranyl acetate and alkaline lead citrate for 15 min consecutively and observed under TEM of Model H-7650 (Hitachi, Ltd., Tokyo, Japan) at 80 kV.

Xenograft tumor model and in vivo imaging by MRI. A total of 20 4-6-week-old female BALB/c nu/nu mice weighing 18-22 g were used for tumor implantation. Sub-confluent SGC-7901 cells were harvested and re-suspended in PBS to a final concentration of $1.0x10^8$/ml. Tumor cell suspension was subcutaneously injected into the flank of each mouse. After 4 weeks, when the subcutaneous mass reached a diameter of 1.0 cm, prior to the development of signs of distress, oxaliplatin-Au-Fe_3O_4-Herceptin NPs complex was injected into the mouse model via the caudal vein at an equivalent iron concentration (0.5 mg/kg). Following 24 h, relaxation time measurements (T_1 and T_2) of an aqueous solution of oxaliplatin-Au-Fe_3O_4-Herceptin and NPs complex *in vivo* were acquired using a clinical magnetic resonance scanner (Signa EXCITE 3.0T HD; GE Healthcare Life Sciences) without contrast. An 11-cm circular coil was used for all the MRI studies. With regards to the T_2-weighted sequence, a repetition time of 750 msec and an echo time of 50-300 msec were employed. To alleviate animal suffering, all mice were euthanized by the end of MRI studies via carbon dioxide asphyxiation followed by cervical dislocation, as the majority of mice become moribund within days of this time point. Subcutaneous tumor masses were harvested and immediately immersed in 10% neutral buffered formalin (pH 6.8-7.2, Thermo Fisher Scientific, Inc.) for 2 h at room temperature and then paraffin embedded and sliced (4 μm).. Iron staining was performed using an iron stain kit (Sigma-Aldrich; Merck KGaA) according to the manufacturer's protocol. Images (magnification, x200) were evaluated with a light microscope (Leica DMi1, Leica Microsystems GmbH, Wetzlar, Germany).

Statistical analysis. Statistical analysis was performed with Student's t-test and one-way analysis of variance using SPSS 10.0 software (SPSS, Inc., Chicago, IL, USA). Bonferroni correction was applied for multiply comparisons dividing the significance level by the number of tested variables. All experiments were performed at least in triplicates and are expressed as the mean ± standard deviation (SD). $P<0.05$ was considered to indicate a statistically significant difference.

Results and Discussion

Synthesis and characterization of Au-Fe_3O_4 NPs. The 8-20 nm Au-Fe_3O_4 NPs were synthesized by decomposing iron pentacarbonyl on the surfaces of Au NPs in the presence of oleic acid and oleylamine. TEM was used to characterize the synthesis of the dumbbell-like Au-Fe_3O_4 NPs. Au NPs were observed as uniform spheres with an average size of 8 nm, based on the size (diameter)-distribution of ~100 NPs. The Au NPs within the Au-Fe_3O_4 NP complexes appeared to be black under TEM images (Fig. 1A) due to the heavy atom effect (27).

Xu *et al* (28) reported the structure of Au-Fe_3O_4 NP in 2009. Compared with conventional single-component Au or Fe_3O_4 NPs, Au-Fe_3O_4 NPs possess unique advantages. First, the structure contains magnetic (Fe_3O_4) and optically active plasmonic (Au) units and can therefore be stably detected optically and magnetically, compared with the fast signal loss observed in common fluorescent labeling. Secondly, the presence of Fe_3O_4 and Au surfaces facilitate the attachment of different chemical functional groups, enabling a variety of target-specific imaging and delivery applications. Thirdly, the size of NPs can be controlled to optimize their magnetic and optical properties, and as small particles are only capable of accommodating a few DNA strands, proteins, antibodies or therapeutic molecules, kinetic cell targeting and drug release assays can be performed (23).

Due to the high surface area-to-volume ratio, NPs have a tendency to aggregate and absorb plasma proteins upon intravenous injection, leading to rapid clearance by the reticuloendothelial system (RES) (29). The size of the Au-Fe_3O_4 NPs in the present study is suitable for *in vivo* applications, as it has been demonstrated that NPs between 10-150 nm in diameter can effectively escape rapid clearance by the RES. NPs are commonly protected with a polymer coating to improve their dispersity and stability (30). In the present study, PEG was used to align the oil phase of the NPs to the water phase, dopamine was reacted with the oleic acid on the

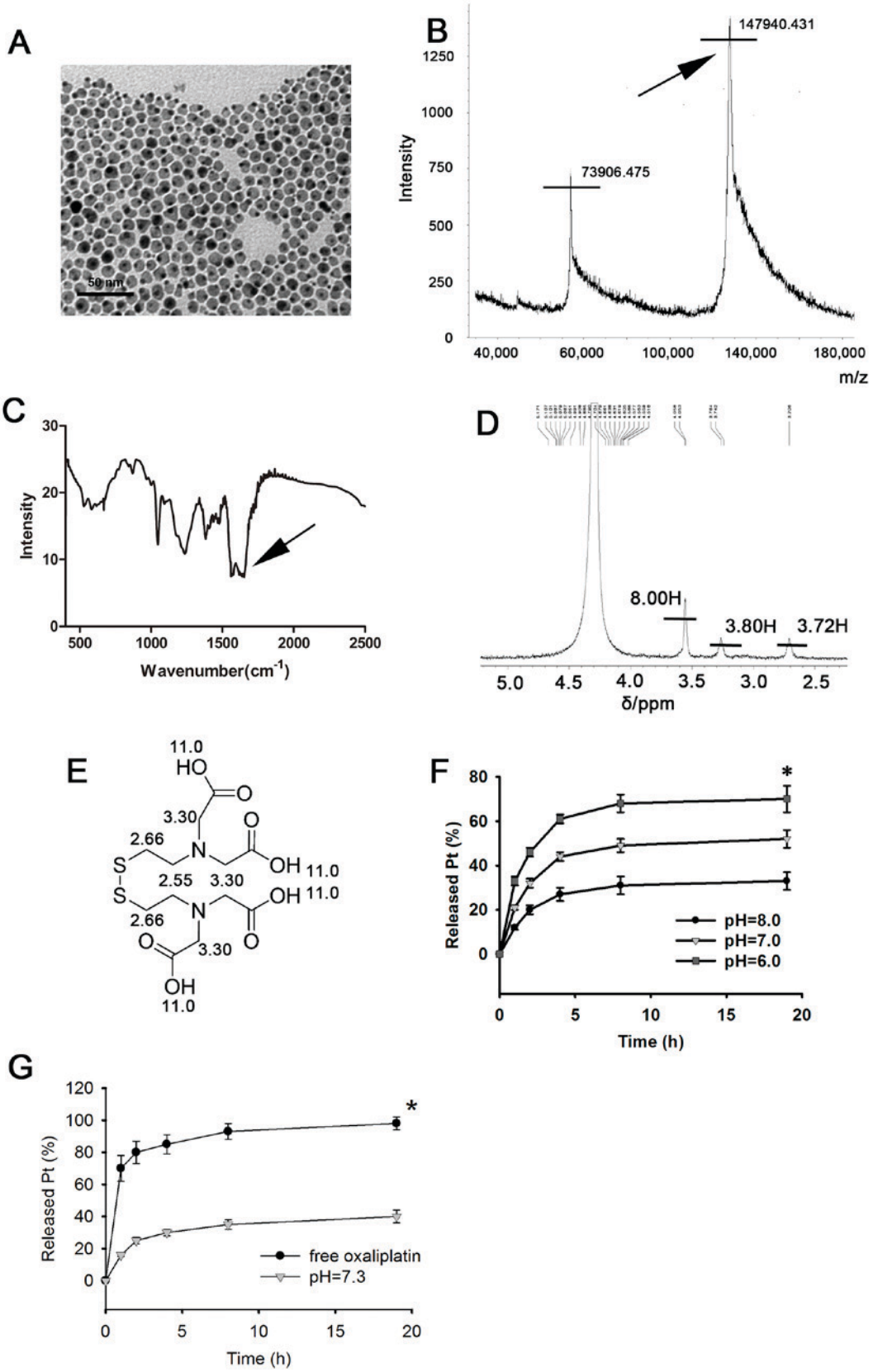

Figure 1. Synthesis and characterization of oxaliplatin-Au-Fe_3O_4-Herceptin NPs. (A) Transmission electron microscope images of dumbbell-shaped structure of 8-20 nm Au-Fe_3O_4 NPs, formed of 8 nm Au NPs (black) and 20 nm Fe_3O_4 NPs (grey). (B) Mass spectrometry analysis of Au-Fe_3O_4-Herceptin NPs. A specific peak for human epithelial growth factor receptor antibody, Herceptin (M_r=148), at *m/z* ~148,000 was detected by matrix-assisted laser-desorption ionization-TOF-TOF. (C) Infrared spectrum of Au-Fe_3O_4-Herceptin NPs. Specific double peaks of carbonyl bands at 1580 and 1650 cm^{-1} (arrow) representing the amide bonds linking the polyethylene glycol to the silane. (D) NMR of the oxaliplatin-binding ligand (D_2O, 300 MHz) revealed peaks at δ 3.51 (8.00 H, s, 3-H), 2.97-3.02 (3.80 H, t, 2-H) and 2.72-2.76 (3.72 H, t, 1-H). (E) The NMR analog of oxaliplatin-binding ligand. (F) The released oxaliplatin level from pH=6.0 group was significantly increased compared with pH=8.0 group. (G) The released oxaliplatin level at pH=7.3 after 4 h of incubation was significantly compared with the free oxaliplatin group. *P<0.01.*P<0.01 vs. pH=8.0. NMR, Nuclear Magnetic Resonance; NPs, nanoparticles; TOF, time of flight; Pt, oxiplatin.

surface of the Fe_3O_4 NPs, then the amino group of dopamine was reacted with the carboxyl group of PEG under catalysis of the EDC-sulfo-NHS system. This ensured that PEG was only connected to the Fe_3O_4 NPs. The ζ-potential of the dumbbell-shaped Au-Fe_3O_4 NPs prior to surface modification was 7.1±1.2 mV. Following being loaded with PEG, the dumbbell-like Au-Fe_3O_4 NPs possessed a ζ-potential of 13.8±1.6 mV. It is notable that the surface charge density of NPs is an important parameter that determines their colloidal stability and cellular interactions (31).

Fe_3O_4 surface functionalization and multifunctional probe loading. Herceptin is a recombinant, DNA-derived, humanized monoclonal antibody glycoprotein that selectively targets the extracellular domain of HER2 (32). Herceptin contains 1,328 amino acids and has a M_r of ~148 (33). Herceptin has been approved for the clinical treatment of HER2-overexpressing breast cancer, metastatic gastric cancer and gastro-esophageal junction adenocarcinoma (34,35). In the present study, the EDC-sulfo-NHS system was used to activate the carboxyl groups of Au-Fe_3O_4 NPs modified with PEG, as aforementioned. Removal of excess EDC and sulfo-NHS prior to addition of Herceptin was used to avoid self-crosslinking of the antibody. Following activation using the EDC-sulfo-NHS system, Herceptin was conjugated to the modified Au-Fe_3O_4 NPs through PEG (M_r=2,000) and dopamine via a condensation reaction with the formation of a peptide bond. Mass spectrometry analysis of oxaliplatin-Au-Fe_3O_4-Herceptin NPs revealed a specific peak for Herceptin at *m/z* ~148,000 (Fig. 1B), which was not detected in Au-Fe_3O_4 NPs. IR spectrum analysis of oxaliplatin-Au-Fe_3O_4-Herceptin NPs revealed the presence of a peptide bond, indicated by specific double split peaks between 1,580-1,650 cm^{-1} (Fig. 1C).

Oxaliplatin has long been used as a chemotherapeutic agent (36); however, it does not specifically target tumor cells and can be taken-up by any rapidly growing cells, leading to toxic side effects (37). The present study proposed that the conjugation of oxaliplatin onto Au-Fe_3O_4-Herceptin NPs, which can actively accumulate in HER2 positive tumor tissues, may greatly decrease the side effects of oxaliplatin. The Au particle of the Au-Fe_3O_4-Herceptin NPs was coated with thiol (HS)-PEG-NH2 with the thiol for oxaliplatin binding. NMR results of the ligand (D_2O, 300 MHz) revealed three peaks at δ 3.51 (8.00 H, s, 3-H), 2.97-3.02 (3.80 H, t, 2-H) and 2.72-2.76 (3.72 H, t, 1-H), as presented in Fig. 1D. The NMR of the analog is depicted in Fig. 1E. Under certain conditions, the disulfide bond of the ligand was broken. One sulfur atom of the ligand was connected to an Au NP and another to oxaliplatin. In the present study, according to the weight percentage of Pt/Au (13.2%), giving a Pt/Au atom ratio of 13:100, ~2,084 Pt units were bound to each Au NP.

The results of drug release profiles *in vitro* at different pH values indicated that oxaliplatin-Au-Fe_3O_4-Herceptin NPs released 13, 21 and 32% of oxaliplatin in the first h and a total of 25, 43 and 58% by 4 h at pH 8.0, 7.0 and 6.0, respectively (P=0.003) (Fig. 1F). It appears that oxaliplatin became more prone to detach from the conjugated NPs in lower pH conditions, and that Pt release is pH dependent. When human serum has a pH of ~7.35, only ~25% of oxaliplatin will be released from the conjugated NPs by 4 h of incubation (28), which delayed the oxaliplatin release by ~4 times compared with free oxaliplatin (80% release, Fig. 1G). However, following uptake by target cells, particularly in the endosomal/lysosomal compartments, which have a pH of ~5.0, >60% of oxaliplatin was released from oxaliplatin-Au-Fe_3O_4-Herceptin NPs (28). This pH dependent release character could reduce the systemic toxicity effect to a great extent and is ideal for the selective targeting therapy *in vivo*.

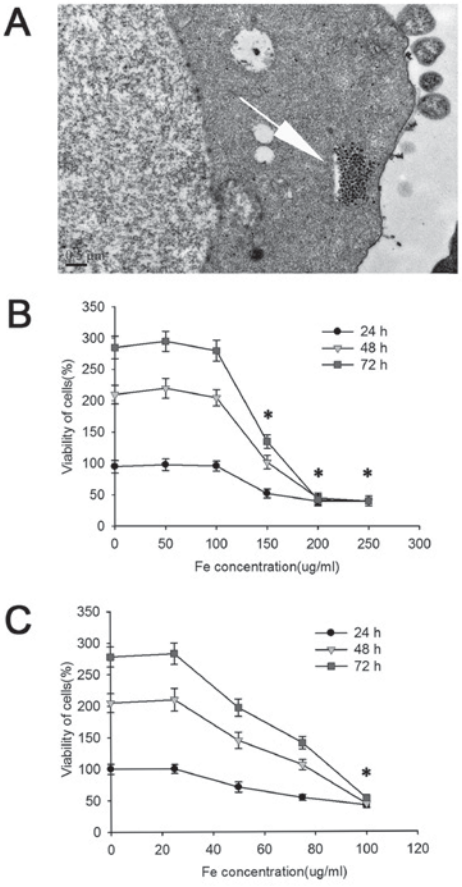

Figure 2. Cellular internalization and cytotoxicity of NPs. (A) Transmission electron microscope image of the oxaliplatin-Au-Fe_3O_4-Herceptin NPs in SGC-7901 cells via endocytosis (arrow) following 2 h incubation. (B) The viability of SGC-7901 cells was not significantly affected until treated with Au-Fe_3O_4 with a Fe concentration >100 μg/ml. (C) The viability of SGC-7901 cells was significantly decreased following incubation with oxaliplatin-Au-Fe_3O_4-Herceptin, compared with control. *P<0.01 vs. 0 μg/ml Fe. NPs, nanoparticles.

Cellular uptake and cytotoxicity of oxaliplatin-Au-Fe_3O_4-Herceptin NPs in SGC-7901 cells in vitro. The SGC-7901 cell line is known to overexpress HER2 and is an ideal cell line to assess the efficacy of HER2 targeted therapy (38,39). Oxaliplatin-Au-Fe_3O_4-Herceptin NPs (0.01 mg/ml Fe) were incubated with SGC-7901 cells for 2 h. TEM image analysis revealed the presence of NPs in the endosome/lysosome, which indicated the successful uptake of NPs through endocytosis (Fig. 2A).

The cytotoxicity of NPs depends on their concentration and the surfactants used (28). In the present study, the water-soluble Au-Fe_3O_4 NPs were tested over a concentration range of 0-250 mg Fe/l. The MTS assay (Fig. 2B) revealed that the Au-Fe_3O_4 NPs did not induce appreciable cell viability (~100%) for ≤100 μg/ml Fe; however, cell viability decreased in a concentration-dependent manner at a Fe concentrations >100 μg/ml, with only half of the cells viable at a Fe

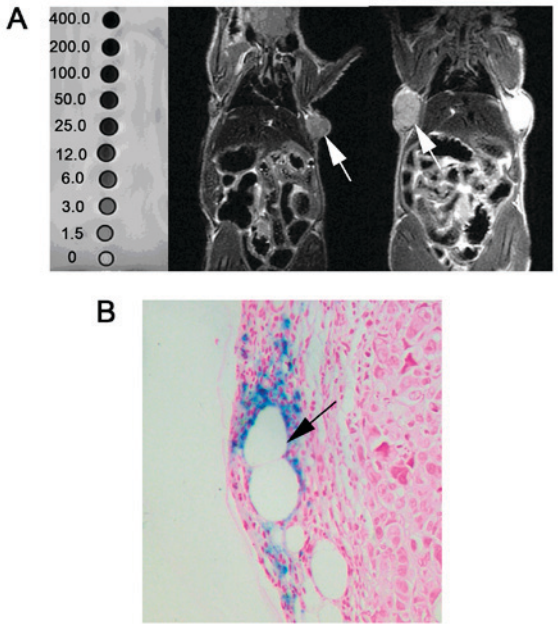

Figure 3. Biodistribution of NPs. (A) T_2-weighted MRI of xenograft tumor mouse model receiving oxaliplatin-Au-Fe_3O_4-Herceptin NPs. Accumulation of the NPs (low signal) was detected inside the percutaneous tumor mass (left arrow), compared with the group treated with Au-Fe_3O_4 NPs alone (right arrow) The color spectrum indicated the association between NPs concentration and the color displayed in T2 MRI. (B) Intracellular iron NPs accumulation around the tumor vessel (arrow) were marked blue using Prussian Blue staining (magnification, x200). NPs, nanoparticles; MRI, magnetic resonance imaging.

concentration of 150 μg/ml (P=0.005). Therefore, within the safe zone (0-100 μg/ml), Au-Fe_3O_4 did not inhibit cell growth and the cytotoxicity of the NPs itself to the tumor cells may be negligible.

The cytotoxicity assays were further performed to assess the effect of oxaliplatin-Au-Fe_3O_4-Herceptin NPs on the viability of HER2-positive SGC-7901 cells *in vitro* (Fig. 2C). The control experiments demonstrated that the cytotoxicity of oxaliplatin-Au-Fe_3O_4-Herceptin NPs was markedly increased compared with Au-Fe_3O_4 NPs (P=0.005). The oxaliplatin-Au-Fe_3O_4-Herceptin NPs had a half-maximal inhibitory concentration toward SGC-7901 cells of 75 μg/ml (Fe concentration). The toxicity was considered to be as a result of two sources, one from Herceptin, the other from oxaliplatin released by hydrolysis.

A variety of specific antigens, including HER2, are frequently overexpressed on the surface of tumor cells. These antigens provide specific targets, which could be selectively bound by monoclonal antibodies. Therefore, when linked to a monoclonal antibody, NP conjugates may enable target-specific delivery via high affinity antibody-antigen interactions and receptor-mediated endocytosis (40-42). A number of cationic NPs have been indicated to enter cells by transiently generating holes in the cell membrane (43). However, most of the uptake of NPs into mammalian cells and macrophages usually occurs via endocytosis (44,45). In the present study, TEM indicated that the platinum-tethered NPs synthesized in the present study were internalized by SGC-7901 cells via endocytosis. Therefore, conjugation of Herceptin to Au-Fe_3O_4 NPs is an effective way for targeted internalization.

Imaging of the selective uptake and accumulation of oxaliplatin-Au-Fe_3O_4-Herceptin NPs in HER2-expressing gastric cancer cells in vivo. The specific targeting efficiency of oxaliplatin-Au-Fe_3O_4-Herceptin NPs with various iron concentrations towards HER2-positive tumor cells was investigated *in vivo* using a xenograft model of SGC-7901 and T_2-weighted MRI without contrast. As depicted in Fig. 3A, the T_2 relaxation time decreased with the increase of the iron concentration in T_2-weighted MRI (Fe concentration of 0.0, 1.5, 3.0, 6.0, 12.0, 25.0, 50.0, 100.0, 200.0, 400.0 μg/ml).

For the purpose of acquiring adequate NPs accumulation at site and a safe dosage for the mice, in the present study, a dose of 0.35 mg/kg Fe was selected for the *in vivo* experiments based on the *in vitro* cytotoxicity assays. A total of 24 h following caudal vein injection, the mice were sodium pentobarbital anesthetized and received MRI examination. In T_2-weighted imaging, the signal intensity of subcutaneous mass was significantly decreased in the oxaliplatin-Au-Fe_3O_4-Herceptin NPs group, compared with the group treated with Au-Fe_3O_4 NPs alone, which demonstrated no detectable intensity alteration. It indicated that the HER2-labeled NPs exhibit increased specificity in their attachment to SGC-7901 cells.

Following the sacrifice, subcutaneous tumor masses were paraffin embedded and stained with Prussian blue. $Fe_4[Fe(CN)_6]_3$ sediment (blue) was then observed around the tumor feeding vascular wall, which indicated oxaliplatin-Au-Fe_3O_4-Herceptin NPs aggregation. These results demonstrated that the oxaliplatin-Au-Fe_3O_4-Herceptin NPs could specifically accumulate in the xenograft tumor mass with HER2 expression via blood flow. The mice were re-imaged by MRI two days following the first scan and no marked signal loss was observed. The study for long term tracking of the NPs *in vivo* remains underway.

Conclusion. In the present study, a dual-functioning NPs conjugate Au-Fe_3O_4 for HER2 targeted oxaliplatin delivery and intracellular drug release triggered via pH was developed. In order to illustrate its targeting and therapeutic potential, cell culture and animal experiments of oxaliplatin-Au-Fe_3O_4-Herceptin NPs against human gastric cancer cell line SGC-7901 were conducted. It was demonstrated that selective targeting of HER2-positive gastric cancer cells using oxaliplatin-Au-Fe_3O_4-Herceptin NPs may increase the efficacy and decrease the side effects of oxaliplatin chemotherapy. Oxaliplatin-Au-Fe_3O_4-Herceptin NPs with high stability in aqueous solution, HER2 targeting, pH dependent drug release and MRI detectable capability were successfully developed in the present study. Evaluation of oxaliplatin-Au-Fe_3O_4-Herceptin NPs *in vivo* by HER2 positive gastric cancer cell line SGC-7901 revealed that NPs demonstrated selective uptake and accumulated in HER2-expressing SGC-7901 xenograft tumor mass, which makes them a promising multifunctional platform for simultaneous magnetic traceable and HER2 targeted chemotherapy for gastric cancer.

Acknowledgements

The authors would like to thank Professor Shouheng Sun of Brown University (Providence, RI, USA) for assisting with the synthesis of Au-Fe_3O_4.

Funding

Zhejiang medical health science and technology plan (grant nos. 2013KYA164 and 2015KYB171), Zhejiang Provincial Natural Science Foundation (grant nos. LY15E010005, LQ15H190001 and LY18H180005).

Availability of data and materials

The datasets used and/or analyzed during the current study are available from the corresponding author on reasonable request.

Authors' contributions

DL managed the experiment design, data collection, animal experiment, MRI analysis and manuscript preparation; XWL and CLC assisted the preparation of Au-Fe_3O_4 NPs and the surface modification. CL, CBZ and WDZ managed the cell culture and assisted the establishment of xenograft tumor model and in vivo imaging. JGZ assisted the animal experiment and MRI analysis. JF and KC in charge of the preparation of Au-Fe_3O_4 NPs, surface modification and ligation of HER2 and oxaliplatin. LC managed the experiment design and manuscript preparation. All authors have approved this manuscript.

Ethics approval and consent to participate

All animal studies were carried out in strict accordance with the guidelines for the welfare and use of animals in cancer research of the Committee of the National Cancer Research Institute. The Zhejiang University Animal Research Committee approved the present study protocol.

Consent for publication

Not applicable.

Competing interests

The authors declare that they have no competing interests.

References

1. Ferlay J, Soerjomataram I, Dikshit R, Eser S, Mathers C, Rebelo M, Parkin DM, Forman D and Bray F: Cancer incidence and mortality worldwide: Sources, methods and major patterns in GLOBOCAN 2012. Int J Cancer 136: E359-E386, 2015.
2. Sato K, Choyke PL and Kobayashi H: Photoimmunotherapy of gastric cancer peritoneal carcinomatosis in a mouse model. PLoS One 9: e113276, 2014.
3. Wagner AD, Unverzagt S, Grothe W, Kleber G, Grothey A, Haerting J and Fleig WE: Chemotherapy for advanced gastric cancer. Cochrane Database Syst Rev 17: CD004064, 2010.
4. Koizumi W, Narahara H, Hara T, Takagane A, Akiya T, Takagi M, Miyashita K, Nishizaki T, Kobayashi O, Takiyama W, *et al*: S-1 plus cisplatin versus S-1 alone for first-line treatment of advanced gastric cancer (SPIRITS trial): A phase III trial. Lancet Oncol 9: 215-221, 2008.
5. Van Cutsem E, Moiseyenko VM, Tjulandin S, Majlis A, Constenla M, Boni C, Rodrigues A, Fodor M, Chao Y, Voznyi E, *et al*: Phase III study of docetaxel and cisplatin plus fluorouracil compared with cisplatin and fluorouracil as first-line therapy for advanced gastric cancer: A report of the V325 Study Group. J Clin Oncol 24: 4991-4997, 2006.
6. Dank M, Zaluski J, Barone C, Valvere V, Yalcin S, Peschel C, Wenczl M, Goker E, Cisar L, Wang K and Bugat R: Randomized phase III study comparing irinotecan combined with 5-fluorouracil and folinic acid to cisplatin combined with 5-fluorouracil in chemotherapy naive patients with advanced adenocarcinoma of the stomach or esophagogastric junction. Ann Oncol 19: 1450-1457, 2008.
7. Cunningham D, Starling N, Rao S, Iveson T, Nicolson M, Coxon F, Middleton G, Daniel F, Oates J and Norman AR; Upper Gastrointestinal Clinical Studies Group of the National Cancer Research Institute of the United Kingdom: Capecitabine and oxaliplatin for advanced esophagogastric cancer. N Engl J Med 358: 36-46, 2008.
8. Tai W, Mahato R and Cheng K: The role of HER2 in cancer therapy and targeted drug delivery. J Control Release 146: 264-275, 2010.
9. Lorenzen S and Lordick F: How will human epidermal growth factor receptor 2-neu data impact clinical management of gastric cancer? Curr Opin Oncol 23: 396-402, 2011.
10. Fornaro L, Lucchesi M, Caparello C, Vasile E, Caponi S, Ginocchi L, Masi G and Falcone A: Anti-HER agents in gastric cancer: From bench to bedside. Nat Rev Gastroenterol Hepatol 8: 369-383, 2011.
11. Pazo Cid RA and Antón A: Advanced HER2-positive gastric cancer: Current and future targeted therapies. Crit Rev Oncol Hematol 85: 350-362, 2013.
12. Shimoyama S: Unraveling trastuzumab and lapatinib inefficiency in gastric cancer: Future steps (review). Mol Clin Oncol 2: 175-181, 2014.
13. Tyagi P and Santos JL: Macromolecule nanotherapeutics: Approaches and challenges. Drug Discov Today: Jan 8, 2018 (Epub ahead of print).
14. Jain TK, Morales MA, Sahoo SK, Leslie-Pelecky DL and Labhasetwar V: Iron oxide nanoparticles for sustained delivery of anticancer agents. Mol Pharm 2: 194-205, 2005.
15. Sun C, Lee JS and Zhang M: Magnetic nanoparticles in MR imaging and drug delivery. Adv Drug Deliv Rev 60: 1252-1265, 2008.
16. Kettering M, Zorn H, Bremer-Streck S, Oehring H, Zeisberger M, Bergemann C, Hergt R, Halbhuber KJ, Kaiser WA and Hilger I: Characterization of iron oxide nanoparticles adsorbed with cisplatin for biomedical applications. Phys Med Biol 54: 5109-5121, 2009.
17. Yang L, Mao H, Cao Z, Wang YA, Peng X, Wang X, Sajja HK, Wang L, Duan H, Ni C, *et al*: Molecular imaging of pancreatic cancer in an animal model using targeted multifunctional nanoparticles. Gastroenterology 136: 1514-1525.e2, 2009.
18. Davis ME, Chen ZG and Shin DM: Nanoparticle therapeutics: An emerging treatment modality for cancer. Nat Rev Drug Discov 7: 771-782, 2008.
19. Tong L, Zhao M, Zhu S and Chen J: Synthesis and application of superparamagnetic iron oxide nanoparticles in targeted therapy and imaging of cancer. Front Med 5: 379-387, 2011.
20. Jain RK and Stylianopoulos T: Delivering nanomedicine to solid tumors. Nat Rev Clin Oncol 7: 653-664, 2010.
21. Fang J, Nakamura H and Maeda H: The EPR effect: Unique features of tumor blood vessels for drug delivery, factors involved, and limitations and augmentation of the effect. Adv Drug Deliv Rev 63: 136-151, 2011.
22. Minchinton AI and Tannock IF: Drug penetration in solid tumours. Nat Rev Cancer 6: 583-592, 2006.
23. Xu C, Xie J, Ho D, Wang C, Kohler N, Walsh EG, Morgan JR, Chin YE and Sun S: Au-Fe3O4 dumbbell nanoparticles as dual-functional probes. Angew Chem Int Ed Engl 47: 173-176, 2008.
24. Stevens WC Jr and Hill DC: General methods for flash chromatography using disposable columns. Mol Divers 13: 247-252, 2009.
25. Workman P, Aboagye EO, Balkwill F, Balmain A, Bruder G, Chaplin DJ, Double JA, Everitt J, Farningham DA, Glennie MJ, *et al*: Guidelines for the welfare and use of animals in cancer research. Br J Cancer 102: 1555-1577, 2010.
26. Gauduchon J, Gouilleux F, Maillard S, Marsaud V, Renoir JM and Sola B: 4-Hydroxytamoxifen inhibits proliferation of multiple myeloma cells in vitro through down-regulation of c-Myc, up-regulation of p27Kip1, and modulation of Bcl-2 family members. Clin Cancer Res 11: 2345-2354, 2005.
27. Imasaka T: Ultraviolet femtosecond laser ionization mass spectrometry. Chem Rec 8: 23-32, 2008.
28. Xu C, Wang B and Sun S: Dumbbell-like Au-Fe3O4 nanoparticles for target-specific platin delivery. J Am Chem Soc 131: 4216-4217, 2009.

29. Cao Z, Zhu W, Wang W, Zhang C, Xu M, Liu J, Feng ST, Jiang Q and Xie X: Stable cerasomes for simultaneous drug delivery and magnetic resonance imaging. Int J Nanomedicine 9: 5103-5116, 2014.
30. Hu Y, Mignani S, Majoral JP, Shen M and Shi X: Construction of iron oxide nanoparticle-based hybrid platforms for tumor imaging and therapy. Chem Soc Rev 47: 1874-1900, 2018.
31. Kim J, Fox C, Peng S, Pusung M, Pectasides E, Matthee E, Hong YS, Do IG, Jang J, Thorner AR, *et al*: Preexisting oncogenic events impact trastuzumab sensitivity in ERBB2-amplified gastro-esophageal adenocarcinoma. J Clin Invest 124: 5145-5158, 2014.
32. Baselga J, Coleman RE, Cortés J and Janni W: Advances in the management of HER2-positive early breast cancer. Crit Rev Oncol Hematol 119: 113-122, 2017.
33. Schneider GF, Subr V, Ulbrich K and Decher G: Multifunctional cytotoxic stealth nanoparticles. A model approach with potential for cancer therapy. Nano Lett 9: 636-642, 2009.
34. Won E, Janjigian YJ and Ilson DH: HER2 directed therapy for gastric/esophageal cancers. Curr Treat Options Oncol 15: 395-404, 2014.
35. Figueroa-Magalhães MC, Jelovac D, Connolly RM and Wolff AC: Treatment of HER2-positive breast cancer. Breast 23: 128-136, 2014.
36. Riddell IA: Cisplatin and Oxaliplatin: Our current understanding of their actions. Met Ions Life Sci 18: pii, 2018. doi: 10.1515/9783110470734-007.
37. Montagnani F, Turrisi G, Marinozzi C, Aliberti C and Fiorentini G: Effectiveness and safety of oxaliplatin compared to cisplatin for advanced, unresectable gastric cancer: A systematic review and meta-analysis. Gastric Cancer 14: 50-55, 2011.
38. Liu K, Chen H, You Q, Shi H and Wang Z: The siRNA cocktail targeting VEGF and HER2 inhibition on the proliferation and induced apoptosis of gastric cancer cell. Mol Cell Biochem 386: 117-124, 2014.
39. Wang T, Zhao J, Ren JL, Zhang L, Wen WH, Zhang R, Qin WW, Jia LT, Yao LB, Zhang YQ, *et al*: Recombinant immunopro-apoptotic proteins with furin site can translocate and kill HER2-positive cancer cells. Cancer Res 67: 11830-11839, 2007.
40. Wang WJ, Lei YY, Mei JH and Wang CL: Recent progress in HER2 associated breast cancer. Asian Pac J Cancer Prev 16: 2591-2600, 2015.
41. Mar N, Vredenburgh JJ and Wasser JS: Targeting HER2 in the treatment of non-small cell lung cancer. Lung Cancer 87: 220-225, 2015.
42. Iqbal N and Iqbal N: Human epidermal growth factor receptor 2 (HER2) in cancers: Overexpression and therapeutic implications. Mol Biol Int 2014: 852748, 2014.
43. Verma A, Uzun O, Hu Y, Hu Y, Han HS, Watson N, Chen S, Irvine DJ and Stellacci F: Surface-structure-regulated cell-membrane penetration by monolayer-protected nanoparticles. Nat Mater 7: 588-595, 2008.
44. López-Castro JD, Maraloiu AV, Delgado JJ, Calvino JJ, Blanchin MG, Gálvez N and Domínguez-Vera JM: From synthetic to natural nanoparticles: Monitoring the biodegradation of SPIO (P904) into ferritin by electron microscopy. Nanoscale 3: 4597-4599, 2011.
45. Lunov O, Zablotskii V, Syrovets T, Röcker C, Tron K, Nienhaus GU and Simmet T: Modeling receptor-mediated endocytosis of polymer-functionalized iron oxide nanoparticles by human macrophages. Biomaterials 32: 547-555, 2011.